17th Mediterranean Conference on Control & Automation
Makedonia Palace, Thessaloniki, Greece
June 24 - 26, 2009

# Switching Losses and Harmonic Currents Evaluation of PWM Techniques for VSI-Fed Dual Stator Induction Motor Drive

Khoudir MAROUANI, Mohamed KHALDI, Farid KHOUCHA, and Abdelaziz KHELOUI
Electrical Engineering Laboratory, Polytechnic Military School
Bordj El-Bahri-16111, Algiers, Algeria
marouani_khoudir@yahoo.fr

*Abstract — In this paper, an analytical evaluation of the harmonic currents and the switching losses in dual stator induction motor (DSIM) drive fed by two three-phase VSIs controlled by PWM techniques is presented. Based on the sine-triangle and space vector PWM techniques concept, eight variants of PWM strategies are presented and compared. So, continuous (CPWM) and discontinuous (DPWM) PWM techniques are obtained according to the selected switching sequences. The analysis is applied to determine the optimal modulation technique that minimizes the switching losses and the rms value of the harmonic currents. It is shown that the CPWM at low modulation and DPWM techniques at the high modulation range have superior performance. Whereas, reduced switching losses are obtained with the DPWM techniques. Therefore, an optimal PWM scheme is obtained with transition between these PWM strategies to allow a performance drive optimization over the whole voltage range.*

*Index Terms — Dual Stator Induction Motor, Continuous Modulation, Discontinuous Modulation, Harmonic Distortion, Switching Losses.*

## I. INTRODUCTION

Nowadays, electrical machine drives are widely used in industrial applications and transportation systems such as electric/hybrid vehicles, traction locomotives and electric propulsion ships, where high-power levels in conjunction with high-performance requirements are more and more demanded. To achieve these high ratings, there are two possible approaches; one focuses on the converter side by increasing the number of output voltage levels and the other one on the machine side by increasing the number of phases. In the first approach, the idea is to divide the high dc bus voltage into multiple low levels and therefore to distribute the high power required among cells of reduced-voltage power switches without the problem of dynamic voltage sharing encountered in the series connection of active devices. However, increasing the number of inverter levels adds to the control complexity and may introduce some voltage imbalance problems. It is a solution well suited for high-power and high-voltage utility applications. For adjustable speed drives, however, an alternative approach is to use a multiphase machine, i.e., a machine with more than three phases in the stator, since the number of phases is not imposed anyway, given that the machine is connected to the electric supply through a dc/ac converter. The number of phases could be used instead as an additional degree of freedom in the overall system design.

Although the answer to the question whether it is better to use a multilevel inverter-fed three-phase machine or a multiphase machine depends on the application, it is undeniable that the latter option offers several advantages which may make it appear very attractive. In fact, the most significant features are a low torque ripple, a reduction in the power per phase and fault-tolerance capability. Other interesting advantages can be pointed out, such as a better torque production per ampere for the same machine volume, higher efficiency and improved reliability. A common type of multiphase machine is the dual stator induction machine (DSIM), where two sets of three-phase windings, spatially phase shifted by 30 electrical degrees, share a common stator magnetic core as shown in Fig.1.

Due to the development of fast switching power semiconductor devices, voltage source inverters (VSIs) are preferred in variable speed machine drives. As VSI-fed multiphase machines are gaining increasing interest for high-power applications, various pulsewidth modulation (PWM) techniques have been developed accordingly, as they strongly affect the overall inverter efficiency and output voltage waveform quality. In a VSI-fed DSIM, the two stator windings are mutually coupled and small unbalances in the two supply voltages may generate high currents. Furthermore, because of the low impedance seen by the voltage harmonic components generated by the switched voltage waveforms, harmonic currents of high level are circulating uselessly in the two stator windings, adding to the overall losses and therefore to the semiconductor devices ratings.

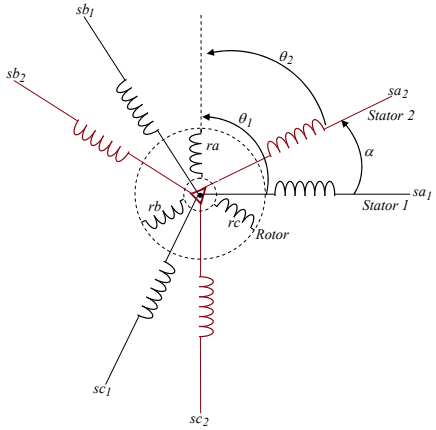


Fig. 1. Dual stator induction machine windings.

## II. Machine Model

The machine model is based on the assumption that space harmonics and magnetic saturation are negligible, and that the two stator three-phase windings are identical and symmetrical with the two neutrals being isolated. In order to derive a practical model suitable for control, the overall machine model is transformed into three decoupled sub models, written in three independent space coordinates, identified as ($\alpha-\beta$), ($x-y$), and ($o1-o2$), respectively [1].

The machine voltage submodel in ($\alpha-\beta$) coordinates can be written as:

$$\begin{bmatrix} vs\alpha \\ vr\alpha \\ vs\beta \\ vr\beta \end{bmatrix} = \begin{bmatrix} Rs & 0 & 0 & 0 \\ 0 & Rr & M\dot{\theta} & Lr\dot{\theta} \\ 0 & 0 & Rs & 0 \\ -M\dot{\theta} & -Lr\dot{\theta} & 0 & Rr \end{bmatrix} \cdot \begin{bmatrix} is\alpha \\ ir\alpha \\ is\beta \\ ir\beta \end{bmatrix} + \begin{bmatrix} Ls & M & 0 & 0 \\ M & Lr & 0 & 0 \\ 0 & 0 & Ls & M \\ 0 & 0 & M & Lr \end{bmatrix} \frac{d}{dt} \begin{bmatrix} is\alpha \\ ir\alpha \\ is\beta \\ ir\beta \end{bmatrix} \quad (1)$$

Where $\dot{\theta} = \Omega m$ is the rotor mechanical speed, and $L$s = $L$ls + 3$L$ms, $L$r = $L$lr + (3/2)$L$mr, $M$ = (3/√2)$M$sr. $L$ls and $L$lr are the stator and rotor leakage inductances in ($\alpha-\beta$) coordinates, respectively. The DSIM ($\alpha-\beta$) submodel expressed in the stationary reference frame is similar to the three-phase induction machine model.

The machine voltage submodel in ($x-y$) coordinates is given by:

$$\begin{bmatrix} vsx \\ vsy \end{bmatrix} = \begin{bmatrix} Rs & 0 \\ 0 & Rs \end{bmatrix} \begin{bmatrix} isx \\ isy \end{bmatrix} + \begin{bmatrix} Lls & 0 \\ 0 & Lls \end{bmatrix} \frac{d}{dt} \begin{bmatrix} isx \\ isy \end{bmatrix} \quad (2)$$

where $L$ls$xy$ is the transformed stator leakage inductance in ($x-y$) coordinates.

The machine voltage submodel in ($o1-o2$) coordinates is expressed as follows:

$$\begin{bmatrix} vso_1 \\ vso_2 \\ vro \end{bmatrix} = \begin{bmatrix} Rs & 0 & 0 \\ 0 & Rs & 0 \\ 0 & 0 & Rr \end{bmatrix} \begin{bmatrix} iso_1 \\ iso_2 \\ iro \end{bmatrix} + \begin{bmatrix} Lls & 0 & 0 \\ 0 & Lls & 0 \\ 0 & 0 & Llr \end{bmatrix} \frac{d}{dt} \begin{bmatrix} iso_1 \\ iso_2 \\ iro \end{bmatrix} \quad (3)$$

where $L$ls$o$ is the transformed stator leakage inductance in ($o1-o2$) coordinates.

The electromagnetic torque of the DSIM is expressed only in terms of stator and rotor ($\alpha-\beta$) current components, since the ($x-y$) and ($o1-o2$) counterparts do not contribute to the electromechanical energy conversion, as shown by (2) and (3). Then, the expression of the electromagnetic torque is then as follows:

$$Ce = pM(is\beta.ir\alpha - is\alpha.ir\beta) \quad (4)$$

where $p$ is the number of pole pairs.

The ($x-y$) and ($o1-o2$) current components do not contribute to the air-gap flux linkages. Hence, they are limited only by the stator resistance and leakage inductance. They produce only losses and therefore must be kept equal to zero or as small as possible.

## III. PWM Control Techniques

Since the dual stator induction motor (DSIM) drive shown in Fig.2 is fed by two three-phase VSIs, the PWM techniques treated in this paper are similar to the one used for the three-phase inverters. So, based on the sine-triangle and space vector PWM techniques concept and according to the selected switching sequences, continuous (CPWM) and discontinuous (DPWM) PWM strategies are presented and compared.

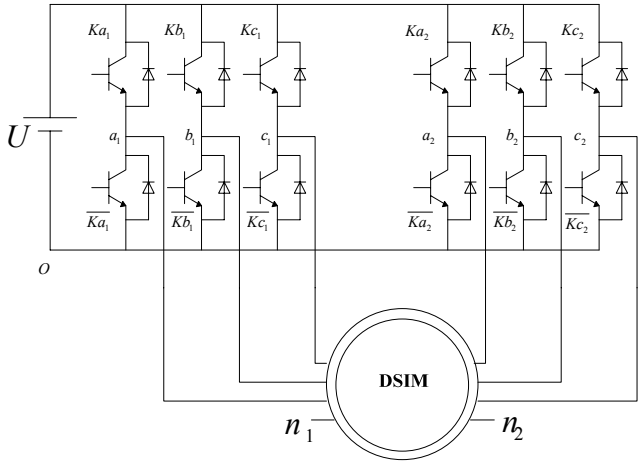


Fig. 2. Six phase VSI fed DSIM.

*1). Sine-Triangle Modulation Technique (STPWM)*

The sine-triangle modulation technique can be extended to the DSIM by shifting the references of the second inverter by 30 electrical degrees. As an example, the three-phase zero-sequence injection modulation technique is presented in Fig.3.

Adding a zero-sequence to the sine-triangle modulation technique can serve to reducing switching losses with different harmonic distortion characteristics. So, in order to reduce switching losses the simplest method is not to switch: the idea was possible using zero-voltage sequences that saturate one of the modulation waves of the three-phases. Although, various zero-sequence signals and therefore modulation strategies can be developed and separated into two groups: continuous (CPWM) and discontinuous (DPWM) PWM strategies.

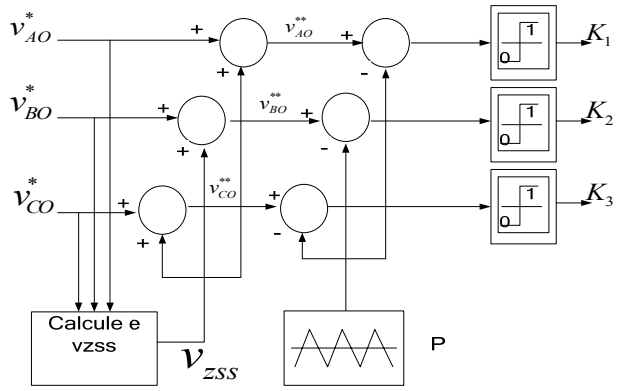


Fig. 3. The generalized signal block diagram of the triangle intersection technique based PWM employing the zero sequence injection principle.

A modulation technique is continuous when on/off switching occurs within every sampling period, for all inverter legs and all sectors. A modulation technique is discontinuous when one (or more) inverter leg stops switching, i.e. the corresponding phase voltage is clamped to the positive or negative dc bus for at least one sector.

A lot of methods gathered under the name of discontinuous PWM (DPWM) have appeared and they differ in the position of saturation level. We can call two-phase modulation the DPWM methods that bring losses reduction. The refereces of the most DPWM modulation techniques can be obtained with the following analytical expressions:

a). DPWM0

$$\left.\begin{array}{l} if\ \left|v_{AO}^*\right| \ge \left|v_{CO}^*\right| \\ and\ \left|v_{BO}^*\right| \ge \left|v_{CO}^*\right| \end{array}\right\} \Rightarrow v_{zss1} = sign\left(v_{AO}^*\right)\frac{U}{2} - v_{AO}^*$$

$$else \qquad v_{zss1} = 0$$

$$\left.\begin{array}{l} if\ \left|v_{CO}^*\right| \ge \left|v_{BO}^*\right| \\ and\ \left|v_{AO}^*\right| \ge \left|v_{BO}^*\right| \end{array}\right\} \Rightarrow v_{zss2} = sign\left(v_{BO}^*\right)\frac{U}{2} - v_{BO}^*$$

$$else \qquad v_{zss2} = 0$$

$$\left.\begin{array}{l} if\ \left|v_{BO}^*\right| \ge \left|v_{AO}^*\right| \\ and\ \left|v_{CO}^*\right| \ge \left|v_{AO}^*\right| \end{array}\right\} \Rightarrow v_{zss3} = sign\left(v_{CO}^*\right)\frac{U}{2} - v_{CO}^*$$

$$else \qquad v_{zss3} = 0$$

$$v_{zss} = v_{zss1} + v_{zss2} + v_{zss3} \qquad (5)$$

b). DPWM1

$$\left.\begin{array}{l} if\ \left|v_{AO}^*\right| \ge \left|v_{BO}^*\right| \\ and\ \left|v_{AO}^*\right| \ge \left|v_{CO}^*\right| \end{array}\right\} \Rightarrow v_{zss1} = sign\left(v_{AO}^*\right)\frac{U}{2} - v_{AO}^*$$

$$else \qquad v_{zss1} = 0$$

$$\left.\begin{array}{l} if\ \left|v_{BO}^*\right| \ge \left|v_{AO}^*\right| \\ and\ \left|v_{BO}^*\right| \ge \left|v_{CO}^*\right| \end{array}\right\} \Rightarrow v_{zss2} = sign\left(v_{BO}^*\right)\frac{U}{2} - v_{BO}^*$$

$$else \qquad v_{zss2} = 0$$

$$\left.\begin{array}{l} if\ \left|v_{CO}^*\right| \ge \left|v_{AO}^*\right| \\ and\ \left|v_{CO}^*\right| \ge \left|v_{BO}^*\right| \end{array}\right\} \Rightarrow v_{zss3} = sign\left(v_{CO}^*\right)\frac{U}{2} - v_{CO}^*$$

$$else \qquad v_{zss3} = 0$$

$$v_{zss} = v_{zss1} + v_{zss2} + v_{zss3} \qquad (6)$$

c). DPWM2

$$\left.\begin{array}{l} if\ \left|v_{AO}^*\right| \ge \left|v_{BO}^*\right| \\ and\ \left|v_{CO}^*\right| \ge \left|v_{BO}^*\right| \end{array}\right\} \Rightarrow v_{zss1} = sign\left(v_{AO}^*\right)\frac{U}{2} - v_{AO}^*$$

$$else \qquad v_{zss1} = 0$$

$$\left.\begin{array}{l} if\ \left|v_{BO}^*\right| \ge \left|v_{CO}^*\right| \\ and\ \left|v_{AO}^*\right| \ge \left|v_{CO}^*\right| \end{array}\right\} \Rightarrow v_{zss2} = sign\left(v_{BO}^*\right)\frac{U}{2} - v_{BO}^*$$

$$else \qquad v_{zss2} = 0$$

$$\left.\begin{array}{l} if\ \left|v_{CO}^*\right| \ge \left|v_{AO}^*\right| \\ and\ \left|v_{BO}^*\right| \ge \left|v_{AO}^*\right| \end{array}\right\} \Rightarrow v_{zss3} = sign\left(v_{CO}^*\right)\frac{U}{2} - v_{CO}^*$$

$$else \qquad v_{zss3} = 0$$

$$v_{zss} = v_{zss1} + v_{zss2} + v_{zss3} \qquad (7)$$

d). DPWM3

$$\left.\begin{array}{l} if\ \left|v_{BO}^*\right| \ge \left|v_{AO}^*\right| \ge \left|v_{CO}^*\right| \\ or\ \left|v_{CO}^*\right| \ge \left|v_{AO}^*\right| \ge \left|v_{BO}^*\right| \end{array}\right\} \Rightarrow v_{zss1} = sign\left(v_{AO}^*\right)\frac{U}{2} - v_{AO}^*$$

$$else \qquad v_{zss1} = 0$$

$$\left.\begin{array}{l} if\ \left|v_{AO}^*\right| \ge \left|v_{BO}^*\right| \ge \left|v_{CO}^*\right| \\ or\ \left|v_{CO}^*\right| \ge \left|v_{BO}^*\right| \ge \left|v_{AO}^*\right| \end{array}\right\} \Rightarrow v_{zss2} = sign\left(v_{BO}^*\right)\frac{U}{2} - v_{BO}^*$$

$$else \qquad v_{zss2} = 0$$

$$\left.\begin{array}{l} if\ \left|v_{BO}^*\right| \ge \left|v_{CO}^*\right| \ge \left|v_{AO}^*\right| \\ or\ \left|v_{AO}^*\right| \ge \left|v_{CO}^*\right| \ge \left|v_{BO}^*\right| \end{array}\right\} \Rightarrow v_{zss3} = sign\left(v_{CO}^*\right)\frac{U}{2} - v_{CO}^*$$

$$else \qquad v_{zss3} = 0$$

$$v_{zss} = v_{zss1} + v_{zss2} + v_{zss3} \qquad (8)$$

e). DPWMAX

$$\left.\begin{array}{l} if\ v_{AO}^* \ge v_{BO}^* \\ and\ v_{AO}^* \ge v_{CO}^* \end{array}\right\} \Rightarrow v_{zss1} = sign\left(v_{AO}^*\right)\frac{U}{2} - v_{AO}^*$$

$$else \qquad v_{zss1} = 0$$

$$\left.\begin{array}{l} if\ v_{BO}^* \ge v_{AO}^* \\ and\ v_{BO}^* \ge v_{CO}^* \end{array}\right\} \Rightarrow v_{zss2} = sign\left(v_{BO}^*\right)\frac{U}{2} - v_{BO}^*$$

$$else \qquad v_{zss2} = 0$$

$$\left.\begin{array}{l} if\ v_{CO}^* \ge v_{AO}^* \\ and\ v_{CO}^* \ge v_{BO}^* \end{array}\right\} \Rightarrow v_{zss3} = sign\left(v_{CO}^*\right)\frac{U}{2} - v_{CO}^*$$

$$else \qquad v_{zss3} = 0$$

$$v_{zss} = v_{zss1} + v_{zss2} + v_{zss3} \qquad (9)$$

f). DPWMIN

$$\left.\begin{array}{l} if\ v_{AO}^* \le v_{BO}^* \\ and\ v_{AO}^* \le v_{CO}^* \end{array}\right\} \Rightarrow v_{zss1} = sign\left(v_{AO}^*\right)\frac{U}{2} - v_{AO}^*$$

$$else \qquad v_{zss1} = 0$$

$$\left.\begin{array}{l} if\ v_{BO}^* \le v_{AO}^* \\ and\ v_{BO}^* \le v_{CO}^* \end{array}\right\} \Rightarrow v_{zss2} = sign\left(v_{BO}^*\right)\frac{U}{2} - v_{BO}^*$$

$$else \qquad v_{zss2} = 0$$

$$\left.\begin{array}{l} if\ v_{CO}^* \le v_{AO}^* \\ and\ v_{CO}^* \le v_{BO}^* \end{array}\right\} \Rightarrow v_{zss3} = sign\left(v_{CO}^*\right)\frac{U}{2} - v_{CO}^*$$

$$else \qquad v_{zss3} = 0$$

$$v_{zss} = v_{zss1} + v_{zss2} + v_{zss3} \qquad (10)$$

The refereces waveform of all these discontinuous PWM strategies are shown in Fig.4.

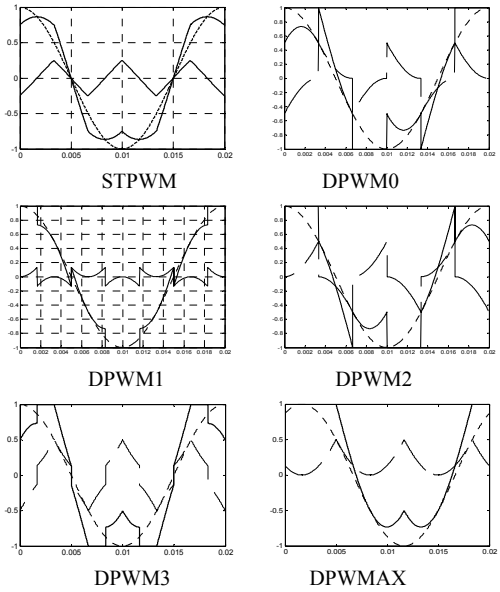


Fig. 4. Modulation waveforms and the zero-sequence signals injected with the STPWM technique.

As we can use only a 120° saturation for each phase reference the difference between two-phase modulation methods consists in choosing the horizon of saturation. DPWM0, DPWM1, DPWM2 are particular cases of GDPWM (Generalized Discontinuous PWM).

As shown in Fig.4, the modulation wave is saturated for 60° every half of the sinusoidal period, but at different angles *y* reported to the initial sinusoidal wave. *y* =0° for DPWM0, *y* =30° for DPWM1 or *y* =60° for DPWM2. The GDPWM method proposes to modulate the angle *y* function of the current phase reported to the voltage wave. This variation can be made only for *y* =0 to 60°. The basic idea is that the saturation must follow the maximum of the line current so that switching wouldn't occur at the time when the line current is high. This insures a losses reduction up to 50% of SVM or three-phase PWM losses.

*2). Space Vector Modulation Technique (SVPWM)*

The switching voltage vectors generated by the three-phase VSI are presented in Fig.5. In conventional SVPWM, the reference voltage vector is synthesized by time average of two adjacent switching vectors and one zero voltage vector in ($\alpha-\beta$) coordinates, as shown in Fig.6.

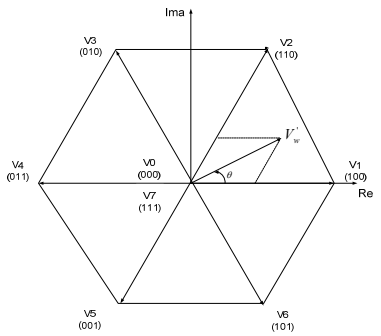


Fig. 5. Representation of the switching state vectors and input reference vector in ($\alpha-\beta$) coordinates.

Each switching vector is switched for its dwell time during the sampling period $T_s$, this dwell time can be calculated from:

$$\begin{bmatrix} T_i \\ T_j \end{bmatrix} = \begin{bmatrix} V_{\alpha i} & V_{\alpha j} \\ V_{\beta i} & V_{\beta j} \end{bmatrix}^{-1} \begin{bmatrix} v_{s\alpha}^* \\ v_{s\beta}^* \end{bmatrix} T_s \qquad (11)$$

$$T_0 + T_7 = T_s - T_i - T_j$$

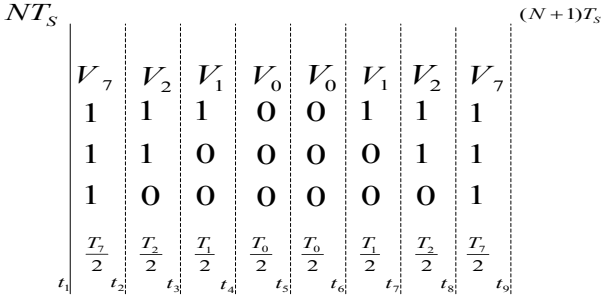


Fig. 6. Switching sequence selection when the reference voltage vector is located in the first sector.

Also, continuous and discontinuous PWM techniques can be obtained with the SVPWM by the distribution of the freewheeling states within the switching sequence. Therefore, the dwell time of the zero voltage vectors can be recalculated as follows:

$$\zeta_0 = \frac{T_0}{T_0 + T_7},\ \zeta_7 = 1 - \zeta_0,\ T_0 = T_7 = \frac{T_s - T_i - T_j}{2} \qquad (12)$$

The distribution of the dwell times $\zeta_7$ and $\zeta_0$ of the freewheeling states is really equivalent to the zero-sequence signals injection modulation technique and as shown in Fig.7, the same discontinuous (DPWM) modulation strategies can be obtained.

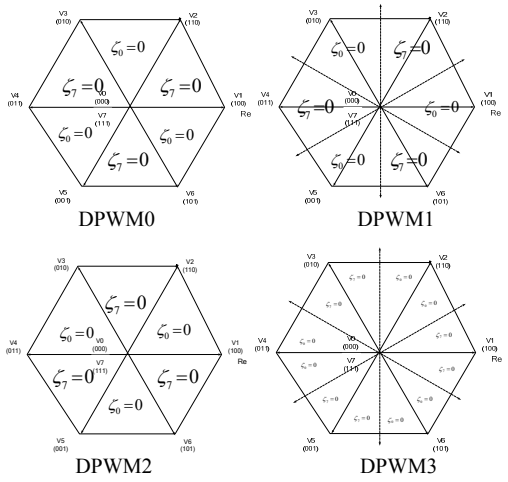


SVPWM : $\zeta_0 = \zeta_7 = 0.5$.

DPWMAX : $\zeta_0 = 0$.

DPWMIN : $\zeta_7 = 0$.

Fig. 7. Distribution of the dwell times $\zeta_7$ and $\zeta_0$ of the freewheeling states. SVPWM, DPWMMAX, and DPWMMIN have space invariant partitioning.

## IV. PERFORMANCE COMPARISON

For comparison purposes, the harmonic current analysis and switching losses evaluation are performed at the same average switching frequency $f_{sw}$ for all the PWM techniques presented in this paper. Therefore, a switching frequency reduction coefficient $k_f$ is introduced for each PWM technique. This coefficient can be determined from the ratio of the discontinuous to the continuous PWM techniques regarding the number of commutations of all legs during one sampling period [1], [3].

### 1). *Harmonic Current Analysis*

The voltage and current waveform quality of the PWM-VSI drives is determined via the switching frequency harmonics, since they determine the switching frequency copper losses and the torque ripple of a motor load and the line current total harmonic distortion of a line-connected VSI. Because, the machine model includes ($\alpha-\beta$) and ($x-y$) components, the harmonic current analysis must be made for the ($\alpha-\beta$) and ($x-y$) currents. The stator voltage equations in the stator coordinate system are expressed as follows:

$$\begin{aligned} v_{s\alpha\beta} &= R_s i_{s\alpha\beta} + \frac{d\lambda_{s\alpha\beta}}{dt} \\ v_{sxy} &= R_s i_{sxy} + L_{lsxy}\frac{di_{sxy}}{dt} \end{aligned} \tag{13}$$

Where the stator and the rotor flux equations are given by:

$$\begin{aligned} \lambda_{s\alpha\beta} &= L_s i_{s\alpha\beta} + M i_{r\alpha\beta} \\ \lambda_{r\alpha\beta} &= L_r i_{r\alpha\beta} + M i_{s\alpha\beta} \end{aligned} \tag{14}$$

If assumed that the reference voltage vector $v^*_{s\alpha\beta}$ is constant over the switching period $T_s$, and that the stator and the rotor time constants are much larger than the switching period, with the resistance drops being neglected [3]. Thus, from (13) and (14), the harmonic voltage equations can be expressed as follows:

$$\tilde{v}_{s\alpha\beta} = \sigma L_s \frac{d\tilde{i}_{s\alpha\beta}}{dt}; \qquad \tilde{v}_{sxy} = L_{lsxy}\frac{d\tilde{i}_{sxy}}{dt} \tag{15}$$

Where $\tilde{v}_{s\alpha\beta}$ is the harmonic voltage and is equal to the difference between the actual voltage vector and the reference vector $v^*_{s\alpha\beta}$.Then, the (α-β) and (x-y) harmonic stator currents per carrier cycle can be calculated as follows:

$$\begin{aligned} \tilde{i}_{s\alpha\beta} &= \frac{1}{\sigma L_s}\int_{NT_s}^{(N+1)T_s}(V_{s\alpha\beta k} - v^*_{s\alpha\beta})dt \\ \tilde{i}_{sxy} &= \frac{1}{L_{lsxy}}\int_{NT_s}^{(N+1)T_s}(V_{sxyk})dt \end{aligned} \tag{16}$$

In (16), $V_{s\alpha\beta k}$ and $V_{sxyk}$ are the inverter output voltage vectors of the $k$th state. In order to eliminate the need for load parameters the harmonic flux trajectories can be investigated. Nevertheless, the (x-y) current components are limited by the stator leakage inductance $L_{lsxy}$, which depends on the coil pitch of the stator windings [1]. Consequently, the harmonic characteristics of the VSI feeding DSIM should be investigated with the introduction of the coefficient $k_{\sigma xy} = \sigma L_s / L_{lsxy}$, which is necessary to evaluate and compare the performances of the PWM techniques. So, employing (16) and normalizing with respect to $\lambda_b$, the per-carrier cycle rms value of the normalized harmonic current can be calculated with:

$$\begin{aligned} \tilde{I}^2_{srms}(m,\theta) &= (\frac{\lambda_b}{\sigma L_s})^2 \frac{1}{T_s}\int_{NT_s}^{(N+1)T_s}(\tilde{\lambda}^2_{s\alpha\beta} + k^2_{\sigma xy}\tilde{\lambda}^2_{sxy})dt \\ &= (\frac{\lambda_b}{\sigma L_s})^2\left(\tilde{\lambda}^2_{s\alpha\beta rms}(m,\theta) + k^2_{\sigma xy}\tilde{\lambda}^2_{sxyrms}(m,\theta)\right) \\ &= (\frac{\lambda_b}{\sigma L_s})^2\left(\tilde{\lambda}^2_{srms}(m,\theta)\right) \end{aligned} \tag{17}$$

where, $\lambda_b = 2\sqrt{3}V_{dc}T_s/\pi$, $\tilde{\lambda}_{s\alpha\beta} = \sigma L_s \tilde{i}_{s\alpha\beta}$, and $\tilde{\lambda}_{sxy} = L_{lsxy}\tilde{i}_{sxy}$

Averaging (17) over a fundamental period results in the global harmonic current calculation as follows:

$$\begin{aligned} \tilde{I}^2_{sfrms}(m) &= (\frac{\lambda_b}{\sigma L_s})^2 \frac{1}{2\pi}\int_{2\pi}\tilde{\lambda}^2_{srms}(m,\theta)d\theta \\ &= (\frac{\lambda_b}{\sigma L_s})^2(\tilde{\lambda}^2_{s\alpha\beta frms}(m) + k^2_{\sigma xy}\tilde{\lambda}^2_{sxyfrms}(m)) \\ &= (\frac{\lambda_b}{\sigma L_s})^2\tilde{\lambda}^2_{sfrms}(m) \end{aligned} \tag{18}$$

The above integral yields a polynomial function of the modulation index $m$. As an example, the per-fundamental cycle rms normalized harmonic flux $\tilde{\lambda}_{sfrms}$ was calculated for the STPWM technique as follows:

$$\begin{aligned} \lambda^2_{\alpha\beta hrms}(m) &= \left(\frac{1}{48}\right)m^2 + \left(-\frac{\left(6+5\sqrt{2}\right)}{18\sqrt{3}\pi^2}\right)m^3 + \left(\frac{1}{4\pi^2}\right)m^4 \\ \lambda^2_{xyhrms}(m) &= \left(-\frac{\left(6+5\sqrt{2}\right)}{18\sqrt{3}\pi^2}\right)m^3 \end{aligned} \tag{19}$$

with: $k_f = \frac{8}{12} = \frac{2}{3}$

The curves of the per-fundamental cycle normalized rms harmonic flux for all the discussed PWM techniques have been plotted as a function of modulation index $m$, as shown in Fig.8. These curves show that the CPWM techniques exhibit the best performance in a low modulation index range, while the DPWM techniques have practically the best performance at the high modulation index range and allow a sampling frequency increase and as a result significant harmonic current reductions can be achieved as shown in Fig.8-(d), for the worst case when $k_{\sigma xy} = 10$.

### *2). Switching Losses Evaluation*

The switching losses of PWM-VSI drive are load current dependent. The inverter per phase model and per carrier cycle switching loss diagram under linear commutation are shown in Fig.9. Firstly, calculating the local switching losses over a sampling period as follows [2-4]:

$$P_{sw} = \frac{1}{T_s}\int_0^{T_s} V_{sw}(t).i_{sw}(t).dt \qquad (20)$$

Then, the total switching losses are calculated by the average value of $P_{sw}$ over the fundamental period as follows:

$$P = \frac{1}{2\pi}\int_0^{2\pi} P_{sw}(t).dt \qquad (21)$$

As an example, the per-fundamental cycle normalized switching losses were calculated for the DPWM1 technique. This results in load power factor angle $\phi$ dependent analytical formula as follows:

$$\begin{cases} \frac{\sqrt{3}}{2}\cos\left(\frac{3\pi}{2}-\phi\right) & -\frac{\pi}{2} \le \phi \le -\frac{\pi}{3} \\ 1-\frac{1}{2}\sin\left(\frac{\pi}{2}-\phi\right) & -\frac{\pi}{3} \le \phi \le \frac{\pi}{3} \\ \frac{\sqrt{3}}{2}\cos\left(\frac{\pi}{2}-\phi\right) & \frac{\pi}{3} \le \phi \le \frac{\pi}{2} \end{cases} \qquad (22)$$

Fig.10-(a), presents the switching losses curves of the discussed DPWM techniques at the same switching frequency. With the CPWM methods, all the phase currents are commutated within each sampling period. Therefore, the switching losses are the same and independent of the load power factor angle. Contrary, Because DPWM techniques cease to switch each switch for a total of 120° per fundamental period, so then the load power factor and the modulation technique together influence the switching losses and contribute to the performance of the drive.

As shown in Fig.10-b, an optimal PWM technique can be obtained with combined DPWM techniques for applications with widely varying power factor conditions.

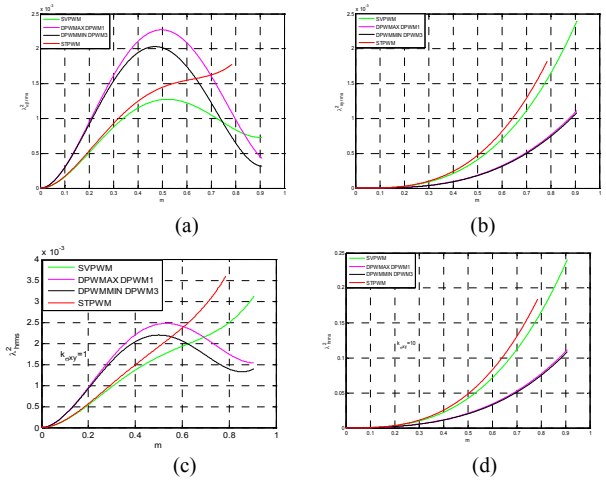


Fig. 8. Per fundamental cycle normalized rms harmonic flux as a function of modulation index *m*, for all the discussed PWM techniques

(a): (α-β) rms harmonic flux. (b): (x-y) rms harmonic flux

(c), (d): rms harmonic flux at different leakage coupling ( $k_{\sigma xy} = 1;10$ ), at the same average switching frequency $f_{sw}$ .

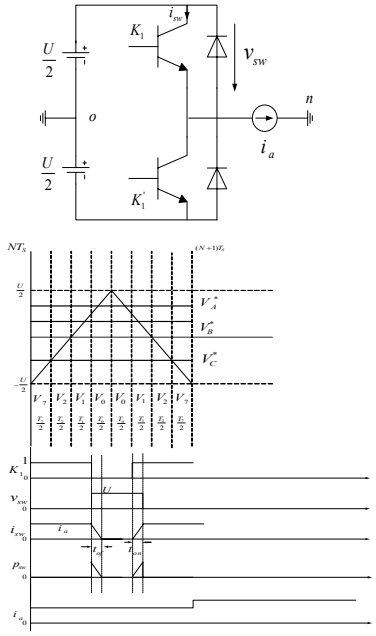


Fig. 9. The inverter per phase model and per carrier cycle switching loss diagram under linear commutation.

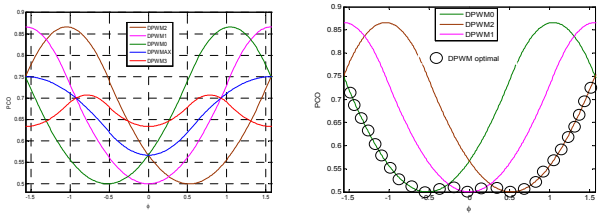


Fig. 10. Switching losses curves of the discussed DPWM techniques at the same switching frequency.

## V. Conclusion

In the present paper, an analytical evaluation of the harmonic currents and the switching losses in dual stator induction motor (DSIM) drive fed by two three-phase VSIs controlled by PWM techniques has been presented. It is shown that the harmonic current rms values vary according to the selected switching sequence and the voltage range. Therefore, the continuous PWM techniques have an advantage in the low voltage range, while the discontinuous PWM strategies are advantageous in the high voltage range with reduced switching losses according to the load power factor angle. Thus, the combination of these strategies contributes to the performance of the drive.

## References


[1] K.Marouani et al., "A New PWM Strategy Based on a 24-Sector Vector Space Decomposition for a Six-Phase VSI-Fed Dual Stator Induction Motor", *IEEE Trans. Ind. Appl.*, vol. 55, no. 5, pp.1910-1920. May 2008.

[2] J. W. Kolar, H. Ertl, F. C. Zach, "Influence of the Modulation Method on the Conduction and Switching Losses of a PWM Converter System", *IEEE Trans. Ind. Appl*, Vol. 27, No. 6, pp. 1063-1075, Nov./Dec. 1991.

[3] A. M. Hava, R. J. Kerkman, T. A Lipo, "Simple Analytical and Graphica Methods for Carrier-Based PWM-VSI Drives", *IEEE Trans. Power Elec.*, Vol. 14, No. 1, pp. 49-61, Jan. 1999.

[4] S. L. CAPITANEANU et al., "Graphical and algebraic synthesis for PWM methods", *EPE Journal,* Vol 11, N°3, Aug. 2001.